



1 **Long-range transport of anthropogenic air pollutants into the**
2 **marine air: Insight into fine particle transport and chloride depletion**
3 **on sea salts**

4 Liang Xu¹, Xiaohuan Liu², Huiwang Gao², Xiaohong Yao², Daizhou Zhang³, Lei Bi¹, Lei Liu¹,
5 Jian Zhang¹, Yinxiao Zhang¹, Yuanyuan Wang¹, Qi Yuan², Weijun Li^{1,*}

6 ¹Department of Atmospheric Sciences, School of Earth Sciences, Zhejiang University, Hangzhou
7 310027, China

8 ²Key Laboratory of Marine Environment and Ecology, Ministry of Education, Ocean University of
9 China, Qingdao 266100, China

10 ³Faculty of Environmental and Symbiotic Sciences, Prefectural University of Kumamoto,
11 Kumamoto 862-8502, Japan

12

13 *Corresponding author: W. Li (liweijun@zju.edu.cn)

14

15 **Abstract**

16 Long-range transport of anthropogenic air pollutants from East Asia can affect the
17 downwind marine air quality during spring and winter. Long-range transport of
18 continental air pollutants and their interaction with sea salt aerosols (SSA)
19 significantly modify the radiative forcing of marine aerosols and influence ocean
20 biogeochemical cycling. Previous studies poorly characterize variations of aerosol
21 particles along with air mass transport from the continental edge to the remote ocean.
22 Here, the research ship R/V Dongfanghong 2 traveled from the eastern China seas



23 (ECS) to the northwestern Pacific Ocean (NWPO) to understand what and how air
24 pollutants were transported from the highly polluted continental air to clean marine air
25 in spring. A transmission electron microscope (TEM) was used to find the long-range
26 transported anthropogenic particles and the possible Cl-depletion phenomenon of SSA
27 in marine air. Primary and secondary anthropogenic aerosols were identified and
28 dramatically declined from 87% to 8% by number from the ECS to remote NWPO.
29 For the SSA aging, 86% of SSA particles in the ECS were identified as fully aged,
30 while the proportion of fully aged SSA particles in the NWPO decreased to 31%. The
31 result highlights that anthropogenic acidic gases in the troposphere (e.g., SO₂, NO_x,
32 and volatile organic compounds) were transported longer distances compared to the
33 anthropogenic aerosol and could exert a significant impact on marine aerosols in the
34 NWPO. These results show that anthropogenic particles and gases from East Asia
35 significantly perturb aerosol chemistry in marine air. The optical properties and cloud
36 condensation nucleation of the modified SSA particles should be incorporated into the
37 more accurately modeling of clouds in the ECS and NWPO in spring and winter.
38



39 **1. Introduction**

40 Marine aerosols play an important role in the global aerosol emission budget and
41 greatly impact the Earth's radiative forcing and biogeochemical cycling (O'Dowd
42 Colin and de Leeuw, 2007). Sea salt aerosol (SSA) is one crucial component of
43 marine aerosols, especially in the remote marine atmosphere (Lewis and Schwartz,
44 2004). SSA is composed of Na and Cl with minor amounts of Mg, Ca, K, and S (Li et
45 al., 2016a). Fresh SSA usually has the form of a cubic NaCl core associated with
46 $MgCl_2$ and $CaSO_4$ coating (Chi et al., 2015). SSA in polluted air can serve as reactive
47 surfaces through the uptake of acidic gaseous SO_2 , NO_x , and organic acids, releasing
48 gaseous reactive chlorine compounds (chloride depletion) (Laskin et al., 2012; Yao
49 and Zhang, 2012). The chloride depletion further releases Cl^- and I-containing
50 compounds into the air which could drive marine new particle formation (He et al.,
51 2021; Yu et al., 2019). Moreover, the SSA aging processes can transform fresh SSA
52 into partially aged SSA and finally into fully aged SSA that mainly contain $NaNO_3$,
53 Na_2SO_4 , and organic sodium salts (Chi et al., 2015; Laskin et al., 2012). These
54 products from the chemical aging processes also modify hygroscopic properties of
55 individual SSA (Cravigan et al., 2020; Ghorai et al., 2014). Some studies found that
56 the aged SSA could alter global climate directly by scattering incoming solar radiation
57 or indirectly by acting as cloud condensation nuclei (CCN) or ice nuclei (IN) in
58 marine air (Hu et al., 2005; Murphy et al., 1998; Pierce and Adams, 2006).

59 It is well known that the interaction of the continental-marine air masses not only
60 releases some active substances into marine air but also supplies many nutrients (e.g.,



61 Fe, N, and P) for biological growth (e.g., plankton) to the ocean's surface (Li et al.,
62 2017; Shi et al., 2012). Some studies have reported that the continental anthropogenic
63 and natural pollutants can be carried to remote marine air through long-range
64 atmospheric transport (Guo et al., 2014; Li et al., 2017; Moffet et al., 2012; Uematsu
65 et al., 2010). The continental pollutants that are deposited into the ocean increase the
66 nutrient input to the seawater, and finally alter the primary productivity in the open
67 sea (Fu et al., 2018; Luo et al., 2016; Mahowald et al., 2018; Shi et al., 2012).
68 Moreover, previous studies found that large amounts of light-absorbing aerosols (e.g.,
69 black carbon and brown carbon) from continental polluted air can be transported into
70 the open ocean air and significantly influence the radiative balance of the marine
71 boundary layer (Kang et al., 2018; Kondo et al., 2016; Ueda et al., 2018; Zhang et al.,
72 2014). Therefore, it is significant to understand the physicochemical properties of
73 continental anthropogenic aerosol particles in marine air.

74 The eastern China seas (ECS: the Yellow Sea and the East China Sea) and the
75 northwestern Pacific Ocean (NWPO) can be affected by the Asian continental air
76 masses under the prevailing westerly winds in winter and spring (Uematsu et al., 2010;
77 Uno et al., 2009). At present, there have been many in-depth studies on the
78 physicochemical properties of aerosols in air masses before they leave the Asian
79 continent. For example, Li et al. (2014) collected aerosol particles at a background
80 site in the Yellow River Delta and determined their physicochemical properties
81 before leaving the Asian continent. Feng et al. (2012) studied the sources and
82 formation pathways of PM_{2.5} at Changdao Island, a resort island in Bohai Sea/Yellow



83 Sea, which is in the transport path of the Asian continental outflow to the Pacific
84 Ocean. Shi et al. (2019) investigated aerosol particles from Asian continental outflow
85 in Qingdao and found the solubility of phosphorus was related to the sources and
86 atmospheric acidification processes. However, these atmospheric field observations
87 were limited to some isolated continental sites.

88 Shipboard observations are an effective way to study marine aerosol properties in
89 remote areas. Using the single particle analysis method (i.e., electron microscope),
90 previous shipboard atmospheric studies have observed chloride depletion and sulfur
91 enrichment in SSA particles from the marine boundary layer (Bondy et al., 2017;
92 McInnes et al., 1994; Mouri and Okada, 1993). At a coastal city in southwestern Japan,
93 Zhang et al. (2003) found that dust particles from Asian continent could mix with SSA
94 particles in the marine atmosphere and further restrained chloride depletion from the
95 sea-salt component in the particles. However, these studies did not examine how
96 anthropogenic pollutants influence the physicochemical properties of SSA from the
97 margin sea air to the remote marine air. Furthermore, they cannot continuously trace
98 the changes of anthropogenic aerosol particles along the pollutants' transport path to
99 the remote NWPO. These information is critical to comprehensively understand the
100 influence of continental anthropogenic air pollutants on the marine air.

101 To achieve this aim, the research ship R/V Dongfanghong 2 was designed to
102 cruise from the ECS to the NWPO so that we could understand what and how air
103 pollutants are transported from the highly polluted continental air to clean marine air
104 in spring. After the cruise, a transmission electron microscope was used to obtain



105 composition, size, morphology, and mixing states of marine aerosol particles. Based
106 on this information, we compared aerosol characteristics over the ECS and the remote
107 NWPO. Furthermore, we also discussed how the continental air masses influence
108 marine aerosols in the ECS and the NWPO air.

109

110 **2. Experiments**

111 **2.1 Aerosol sampling and analyses**

112 Aerosol samples were collected on board the R/V Dongfanghong 2 during the
113 cruise from 17 March to 22 April 2014. The cruise path crossed the ECS and the
114 NWPO (Figure 1). Aerosol particles were sampled onto copper TEM grids (carbon
115 type-B, 300-mesh copper; Tianld Co., China) using a DKL-2 sampler (Genstar
116 Electronic Technology, China). The sampler was equipped with a single-stage
117 impactor with a 0.5 mm diameter jet nozzle at an airflow of 1.0 L/min. If the particle
118 density is 2 g cm^{-3} , the collection efficiency of the sampler is 50% for particles with a
119 260 nm aerodynamic diameter. All the samples were collected at the ship's bow to
120 avoid contamination from the exhaust. During the same cruise, the short-period
121 contribution from contamination of particulate matter was less than 3% (Luo et al.,
122 2016). The sampling duration varied from 2 to 3 min to avoid individual particles
123 overlap on the substrate. After the collection, all the samples were sealed in dry plastic
124 capsules and stored in a desiccator at $25 \text{ }^\circ\text{C}$ and $20 \pm 3\%$ relative humidity (RH) for
125 further analysis.

126 The aerosol particles were analyzed by a JEOL JEM-2100 transmission electron



127 microscope (TEM) operated at 200 kV. The chemical elements (heavier than carbon,
128 $Z \geq 6$) were semi-quantitatively detected by an energy-dispersive X-ray spectrometer
129 (EDS) (Oxford Instruments, UK). The iTEM software (Olympus Soft Imaging
130 Solutions GmbH, Germany) was used to analyze individual particles in the TEM
131 images and obtain their projected area, perimeter, aspect ratio, and equivalent circle
132 diameter (ECD).

133 A total of 22 samples were analyzed in this study. The location of each sample is
134 shown in Figure 1. The details about sampling dates, times, and meteorological
135 conditions for each sample are listed in Table S1. Due to the influence of the
136 westerlies, the ECS is frequently affected by the air pollutants' transport from Asiain
137 spring (Shi et al., 2019). The NWPO is less affected by the transport of continental
138 pollutants because of the remote distance (Zhang et al., 2018). According to the
139 sample locations, we defined two sample categories along with the cruise path (Figure
140 1): 11 samples in the ECS and 11 samples in the NWPO.

141 2.2 Air mass backward trajectories

142 The NOAA HYSPLIT (Hybrid Single Particle Lagrangian Integrated Trajectory)
143 trajectory model (Stein et al., 2015) was applied to calculate the backward trajectories
144 for the investigation of air mass sources and transport paths. The total run time was
145 set at 48 hours. We selected an altitude of 500 m as the endpoint in each backward
146 trajectory. In this study, we obtained 21 backward trajectories.

147

148 3. Results



149 **3.1 Classification and relative abundance of aerosol particles**

150 The TEM analyses provided the morphology, mixing state, and composition of
151 individual particles. In this study, we analyzed 3,734 particles in 22 samples (2,770
152 particles collected in the ECS and 964 particles in the NWPO). Aerosol particles were
153 classified into seven types based on their composition and morphology: sulfur-rich
154 (S-rich), organic matter (OM), soot, metal, fly ash, mineral, and sea salt. S-rich
155 particles are considered as secondary inorganic particles (e.g., $(\text{NH}_4)_2\text{SO}_4$ and
156 NH_4NO_3), which are formed from their gaseous precursors, such as SO_2 , NO_x , and
157 NH_3 . OM particles mainly contain C and certain O and Si. Here we observed two
158 kinds of OM particles: spherical or irregular primary organic matter (POM) particles
159 and secondary organic matter (SOM) particles. The POM is directly emitted from the
160 combustion of fossil fuel and biomass and SOM is formed from volatile organic
161 compounds (VOCs) or the oxidized POM in the atmosphere (Li et al., 2016a; Wang et
162 al., 2021). The SOM is normally mixed with S-rich particles (Li et al., 2016b). Soot
163 particles (i.e., black carbon) are chain-like aggregates of carbonaceous spheres,
164 mainly containing C and minor O. Metal particles mainly contain Fe, Zn, and Pb, and
165 fly ash particles contain Si, Al, and minor Ca and Fe. Metal and fly ash particles both
166 display spherical shapes and are directly emitted from heavy industrial activities such
167 as power plants and steel factories (Li et al., 2017). Mineral particles are composed of
168 Si, Al, Ca, and Fe and present irregular shapes (Figure 2a). Mineral particles originate
169 from arid deserts (e.g., Sahara and Gobi), roads, and construction activities in the
170 continental areas. Sea salt aerosol (SSA, Figure 2b) is from the bursting of air bubbles



171 resulting from the waves breaking. SSA is mainly composed of Na and Cl, with minor
172 Mg, Ca, K, and S.

173 The high-resolution TEM could see through the thin materials on the substrate, so
174 the inner mixing structure of different aerosol components in individual particles can
175 be directly identified (Li et al., 2016b; Riemer et al., 2019). We found that most of the
176 individual non-SSA particles collected in marine air contained two or more different
177 types of anthropogenic aerosols. To elucidate the mixing structure of the non-SSA
178 particles, we further defined six types of non-SSA particles: S-metal (Figure 2c), S-fly
179 ash (Figure 2d), S-soot (Figure 2e), OM coating (Figure 2f), OM-S (Figure 2g), and
180 S-rich (Figure 2h). In the ECS, anthropogenic aerosols accounted for 87% of all
181 particles by number fraction, including S-rich for 42 %, S-soot for 21%, S-metal/fly
182 ash for 8%, OM-S for 6%, and OM coating for 10%. Only 8% of the observed
183 particles in the ECS were SSA particles. The remaining 5% was identified as mineral
184 particles. Interestingly, SSA particles became the dominant aerosol at 90% in the
185 NWPO and anthropogenic aerosols only accounted for 8%, suggesting that marine
186 emissions became the primary aerosol source in the NWPO. Therefore, there are large
187 differences between aerosol particles in the ECS and the NWPO (Figure 3).

188

189 **3.2 Variations of aerosol particles from the ECS to the NWPO**

190 Figure 3 shows variations of aerosol particles along with the cruise pathway from
191 the ECS to the NWPO. Mineral particles can only be transported from continental
192 areas. Figure 3 shows that higher number fractions of mineral particles always



193 occurred when the sampling sites were close to eastern China. The number fraction of
194 mineral particles rose to 15% in the coastal air during the cruise (Figure 3). The
195 proportion of mineral particles decreased from 15% to 3% for the samples collected in
196 the ECS. When the ship traveled eastward into the NWPO, the proportion of mineral
197 particles dropped to a low level (2%). In contrast, the proportion of mineral particles
198 increased again when the ship returned to the ECS. Altogether, the number fraction of
199 mineral particles was 5% in the ECS, twice as high as that in the NWPO, suggesting
200 that the ECS and NWPO were influenced by westerlies during the sampling period.
201 Indeed, Figure 1 shows that most of 48h backward trajectories of air masses in the
202 ECS were sourced from eastern China and that some of the 48h back trajectories of air
203 masses in the NWPO crossed Japan.

204 Figure 3 shows that S-metal and S-fly ash (two typical anthropogenic aerosol
205 particles) displayed variation similar to the mineral particles. Number fractions of
206 S-metal and S-fly ash particles in the ECS samples ranged from 17% to 2% with the
207 average value at 8%, but only 0.3% for S-metal and S-fly ash particle was found in
208 the NWPO. In a word, we conclude that aerosol particles from the Asian continent
209 directly exert much greater impacts on the ECS than the NWPO.

210 **3.3 Comparison of anthropogenic secondary aerosol particles**

211 Secondary S-rich and OM coating particles are normally considered as arising
212 from the conversion of anthropogenic gaseous pollutants (e.g., SO₂, NO_x, NH₃, and
213 VOCs) (Li et al., 2021). TEM observations clearly identified secondary particles and
214 showed their variation of number fraction in the samples (Figure 3). Our results show



215 that number fractions of S-rich particles were dominant in the ECS samples with the
216 range of 32%-71%, but their fractions decreased to 5% in the NWPO. The results
217 indicate that secondary particles in the ECS were strongly influenced by
218 anthropogenic pollutants transported from eastern China. Furthermore, we noticed
219 that secondary aerosol particles were frequently mixed with some typical fine primary
220 anthropogenic particles (e.g., soot, fly ash, and metal) and formed S-soot/S-fly
221 ash/S-metal particles (Figure 4). As a result, we conclude that the anthropogenic gases
222 or aerosol pollutants in the continental air masses significantly influence the
223 downwind air quality of the ECS, but they have a minor impact on the NWPO air.

224 It should be noted that OM coating particles were frequently found in the ECS but
225 barely observed in the NWPO. In other words, S-rich particles in the NWPO had no
226 typical OM coating, although S-rich particles accounted for ~5% in the NWPO
227 samples. Figure 4b shows that these S-rich particles in the NWPO only had one
228 dominant size range smaller than 1 μm , which is different from the larger and broader
229 size distribution of S-rich particles in the ECS. In addition, we noticed the particularly
230 high fraction of S-rich particles in Sample #11 and #12 collected in the NWPO (15%
231 and 24%). These results indicate that these S-rich particles likely formed in the
232 NWPO air. Coincidentally, Zhu et al. (2019) observed a new particle formation event in
233 the same area and proposed that the event was likely caused by long-range transported
234 continental gases (e.g., SO_2 , NO_x , and VOCs).

235 **3.4 Aging of sea salt aerosols**

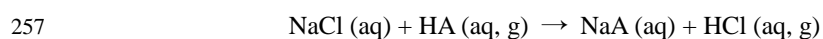
236 As the dominant aerosol particles in marine air, SSA particles accounted for



237 70%-98% in the NWPO. SSA could serve as reactive surfaces for heterogeneous and
238 multiphase chemical reactions in the atmosphere, and these reactions also could alter
239 the morphology and composition of SSA (Athanasopoulou et al., 2008; Chi et al.,
240 2015; Laskin et al., 2012). Based on the morphology and composition of SSA, we
241 further classified SSA into three categories: fresh SSA, partially aged SSA, and fully
242 aged SSA (Figure 5).

243 The fresh SSA did not experience any chemical modification in the atmosphere.
244 TEM images of fresh SSA indicate the cubic NaCl core and coating composed of
245 MgCl₂ and CaSO₄ (Figure 5a). The NaCl core only contains Na and Cl, with the
246 atomic ratio of Na to Cl close to 1:1 (Figure 5d). The major components in the coating
247 are Mg, O, S, Cl, and Ca (Figure 5e), thus, we infer their molecular forms as MgCl₂
248 and CaSO₄ (Buseck and Pósfai, 1999; Chi et al., 2015; Geng et al., 2010; Pósfai et al.,
249 1994).

250 The partially aged SSA represent those SSA particles that undergo chemical
251 modification but still retain part of the NaCl core (Figure 5b). The morphological
252 differences can be observed between the fresh SSA and partially aged SSA. The NaCl
253 core still persists in the partially aged SSA but cannot keep its regular cubic shape.
254 Meanwhile, the coating composition turns into O, Na, Mg, Ca, and S, with decreasing
255 Cl (Figure 5f). The SSA aging is attributed to the Cl-depletion phenomena, which can
256 be expressed as follows (Laskin et al., 2012):



258 where HA represent atmospheric acids (e.g., H₂SO₄, HNO₃, and methanesulfonic



259 acid). NaCl in the SSA could react with inorganic (e.g., HNO₃ and H₂SO₄) or organic
260 acid (e.g., methanesulfonic acid), releasing volatile HCl (g) to the atmosphere, leading
261 to depletion in chloride and enrichment in corresponding sodium salts.

262 We define the fully aged SSA as particles whose NaCl cores have been
263 completely transformed into NaNO₃ and Na₂SO₄. Figure 5c shows that the NaCl cores
264 in the fully aged SSA entirely disappeared, leaving a rounder shape. The Cl element
265 was no longer detected in the fully aged SSA and the major aerosol components were
266 the mixture of NaNO₃ and Na₂SO₄ (Figure 5g).

267 To evaluate composition differences of SSA, we present triangular diagrams of
268 Na-Cl-S weight ratio based on the EDS. Figure 6a shows that the fresh SSA is around
269 the NaCl, the partially aged SSA is distributed in the center of triangular, and the fully
270 aged SSA is around NaNO₃ and Na₂SO₄. Figure 6b shows that there were large
271 variations of the SSA components in the ECS and NWPO. Our results show that most
272 of the aged SSA in the ECS were the mixture of NaNO₃ and Na₂SO₄, suggesting that
273 SSA in the ECS underwent heterogeneous reactions and become fully aged SSA. SSA
274 in the NWPO is widely distributed between NaCl and NaNO₃/Na₂SO₄ in the
275 triangular diagram, suggesting that these were partially aged SSA particles.

276 Figure 7 shows the relative abundance of SSA at different sampling sites from the
277 ECS to the NWPO. In the ECS, 86% of SSA particles were fully aged. As the ship
278 traveled into the NWPO, fully aged SSA particles decreased to 31%, meanwhile the
279 proportion of fresh SSA increased to 55%. The size distribution of SSA particles
280 shows that the proportion of fresh SSA increased with the increase of particle size



281 from 0.05 to 5 μm (Figure 8). On the contrary, the proportion of fully aged SSA
282 decreased with the increase of particle size from 0.05 to 5 μm . Overall, partially and
283 fully aged SSA accounted for 61% of SSA particles smaller than 3 μm , while fresh
284 SSA dominated (81%) in SSA particles larger than 3 μm . Figure 8 also reveals that 94%
285 of the fully aged SSA particles were smaller than 3 μm .

286

287 **4. Discussion**

288 Abundant BC, metal, and fly ash particles in the ECS show that long-range
289 transport of anthropogenic aerosol particles from the polluted continental areas
290 constantly influence the ECS air during the spring and winter. Moreover, the existence
291 of OM coating particles (10%, Figure 3) in the ECS indicates that secondary
292 sulfate/nitrate particles underwent aging process and formed the OM coating during
293 their transport (Li et al., 2021). This result suggests that the long-range transported air
294 masses from continental areas brought abundant anthropogenic gases such as NO_x ,
295 SO_2 , and VOCs into marine air. Indeed, the HYSPLIT backward trajectories show
296 that the air masses in the ECS were mainly from eastern China (Figure 1). Under the
297 influence of the westerlies, a large number of anthropogenic and natural pollutants are
298 transported to the ECS and further influence its air quality.

299 Figure 3 shows that both primary and secondary anthropogenic aerosols were
300 relatively low in the NWPO (8%), suggesting a slight influence from continental
301 aerosols. However, we observed severe Cl-depletion in SSA in some samples in the
302 NWPO. The Cl-depletion of SSA is mainly caused by the heterogeneous reactions



303 with acidic gaseous pollutants in marine air (Chi et al., 2015; Hsu et al., 2007; Laskin
304 et al., 2012). By comparing the aging degree of SSA and air mass backward
305 trajectories, we found that the air masses with a relatively high proportion of fully
306 aged SSA particles (#13 and #15) mostly formed due to the anthropogenic gaseous
307 pollutants (e.g., SO₂ and NO_x) from northwest China and Japan (Figure S1). The
308 result suggests that aerosol particles and gases might have different transport distances.
309 Aerosol particles could be significantly removed by dry or wet deposition. However,
310 the anthropogenic gases can be transported further to the NWPO air (Figure 9). Over
311 the western Pacific, Koike et al. (2003) also found that anthropogenic gaseous
312 pollutants (e.g., NO_x and SO₂) from the East Asia have higher transport efficiency
313 than aerosols from the same region. Meanwhile, the surface changes of SSA can be
314 considered as a potential indicator for anthropogenic gaseous pollutants in remote
315 marine air.

316 Figure 6 shows a higher percentage of Cl-free SSA particles (on Cl = 0 line) in
317 the ECS than those in NWPO, suggesting modifications of SSA in the ECS were
318 much more severe than them in the NWPO. Referred to Zhang et al. (2003), we
319 further provide the dash line that Na:Cl:S was changed only by reaction with H₂SO₄.
320 Thus, particles above the dash line represent that Cl in these SSA particles was
321 replaced by S deposition and other chemical processes (e.g., HNO₃ and organic acids).
322 The number of fully aged SSA particles above the dash line was further counted.
323 Surprisingly, we found that Cl-depletion in 70% of the fully aged SSA particles in the
324 ECS was not only caused by S deposition, but the fraction increased to 87% in the



325 NWPO (Figure 6). The result indicates that a higher proportion of the fully aged SSA
326 particles in the NWPO were reacted with diverse acids besides H₂SO₄.

327 It is well known that organic acids could also be a reason of Cl-depletion in SSA
328 (Chi et al., 2015; Laskin et al., 2012). It is well known that the oxidation of dimethyl
329 sulfide (DMS) emitted from phytoplankton contributes to the Cl-depletion in SSA
330 (Sievering et al., 2004). Both anthropogenic acid gases and DMS in the ECS were
331 found to be higher than that in the NWPO (Figures S1 and S2). Compared with the
332 ECS, we found that DMS in our NWPO shipping area had lower mass concentrations
333 and minor fluctuations ($3\text{--}6 \times 10^{-11} \text{ kg m}^{-3}$, Fig S2). However, the percentages of aged
334 SSA differed widely (from 23% to 91%) within the NWPO. We deduce that the low
335 concentration of the DMS only slightly modified part of SSA in the NWPO, but it was
336 not enough to influence all the SSA. Moreover, Zhu et al. (2019) reported that
337 secondary sulfate particles in the NWPO were mostly came from the long-range
338 transported acidic gases during the sampling period. The contribution of DMS to
339 non-sea-salt sulfate is less than 6% in the remote ocean of the northern hemisphere
340 (George et al., 2008; Quinn et al., 1990; Savoie et al., 1994). Therefore, a large
341 proportion of aged SSA particles in the NWPO should be mainly attributed to the
342 anthropogenic acidic gases from long-range transport.

343 Previous studies found that SSA emissions increased with the increase of wind
344 speed (Feng et al., 2017; Pant et al., 2008; Shinozuka et al., 2004). In our study, the
345 proportion of fresh SSA increases with increasing wind speed (Figure 7), consistent
346 with the aforementioned studies. SSA particles of a smaller size have lower dry



347 deposition velocities and longer lifetimes in the air (Lewis and Schwartz, 2004),
348 which could enhance the Cl-depletion. This could be the reason that partially and fully
349 aged SSA was mostly in the smaller size range ($<3 \mu\text{m}$) (Figure 8). On the contrary,
350 the newly emitted coarse SSA particles with high dry deposition velocity are more
351 likely to deposit to the ocean, resulting in less reacted SSA. As a result, the fresh SSA
352 from local sea spray was mostly found in the coarse size range (larger than $3 \mu\text{m}$) in
353 our samples (Figure 8). This result suggests that it is crucial to study aging process
354 among the size-resolved SSA, especially particles smaller than $3 \mu\text{m}$.

355 In the future, we need to pay more attention to the influence of anthropogenic
356 gaseous pollutants on the SSA aging in remote marine air. On the one hand, the aging
357 processes could modify the hygroscopicity of SSA, determining their morphology and
358 phase state in the humidified marine environment, in the end directly affecting optical
359 properties of SSA (Wang et al., 2019). On the other hand, the hygroscopicity change
360 due to SSA aging could alter CCN activity, and indirectly affect global climate (Hu et
361 al., 2005; Murphy et al., 1998; Pierce and Adams, 2006). The SSA aging processes
362 could release more Cl- and I-containing compounds into air, which might lead to
363 marine new particle formation and growth (He et al., 2021). Meanwhile, the SSA also
364 serves as an important sink for the anthropogenic acidic gases in remote marine areas
365 (Chi et al., 2015; Laskin et al., 2012). Thus, in future research, it would be crucial to
366 quantify the anthropogenic acidic gases scavenged by SSA.

367

368 **5. Conclusions**



369 Individual aerosol particles were collected from 17 March to 22 April, 2014 on
370 board of the ship R/V Dongfanghong 2 from the ECS to the NWPO. We classified
371 aerosol particles based on their composition, morphology, and mixing state: mineral,
372 sea salt, S-metal, S-fly ash, S-soot, OM coating, OM-S, and S-rich. Microscopic
373 analysis showed that anthropogenic aerosols accounted for 87% of the total particle
374 number in the ECS. In particular, higher proportions of secondary particles (i.e.,
375 S-rich particles, 42%, and OM coating particles, 10%) were found in the ECS.
376 Meanwhile, primary and secondary anthropogenic aerosols are relatively low in the
377 NWPO (8%).

378 TEM observations revealed that SSA particles were the most abundant in the
379 NWPO atmosphere, accounting for 90% of all analyzed aerosol particles. The
380 Cl-depletion of sea salt aerosol (SSA) particles caused by the heterogeneous reactions
381 with acidic gaseous pollutants was further observed. Three types of SSA particles,
382 fresh, partially aged, and fully aged were classified. Fully aged SSA particles were the
383 dominant SSA in the ECS (86%), while fully aged SSA particles decreased to 31% in
384 the NWPO. The severe aging of SSA (partially and fully aged, at most 88% of SSA)
385 was still found in the NWPO, despite there being only minor anthropogenic aerosol
386 particles. These results show that aerosol particles from the continent air might be
387 removed by dry and wet deposition, but the air pollutants were transported further to
388 the NWPO. The aging of SSA particles has important effects on their hygroscopic and
389 optical properties, one effect being the promotion of heterogeneous reaction with
390 acidic gases in the NWPO. Our observations show that more attention should be given



391 to the influence of anthropogenic gaseous pollutants on the Cl-depletion on SSA in
392 remote marine areas.

393

394 **Supplement**

395 The supplement related to this article is available online at:

396

397 **Author contributions**

398 LX and WL conceived the study and wrote the article. The sampling during the
399 research cruise was organized by XL, HG, and XY. LX, WL, LL, JZ, YZ, YW, and
400 QY carried out TEM analyses of individual particles. DZ and LB contributed to the
401 improvement of this paper. All authors reviewed and approved the paper.

402

403 **Competing interests**

404 The authors declare that they have no conflict of interest.

405

406 **Acknowledgements**

407 We thank Peter Hyde for his editorial comments. We acknowledge the NOAA Air
408 Resources Laboratory for the provision of the HYSPLIT transport and dispersion
409 model and READY website (<http://www.ready.noaa.gov>) used in this publication.

410

411 **Financial support**

412 This research was supported by the National Natural Science Foundation of China



413 (grant nos. 42075096, 91844301, and 41807305), the National Key R&D Program of
414 China (grant no. 2017YFC0212700), Zhejiang Provincial Natural Science Foundation
415 of China (grant no. LZ19D050001), and China Postdoctoral Science Foundation
416 (grant no. 2019M662021).

417

418 **References**

- 419 Athanasopoulou, E., M. Tombrou, S. N. Pandis, and A. G. Russell (2008), The role of sea-salt
420 emissions and heterogeneous chemistry in the air quality of polluted coastal areas, *Atmospheric*
421 *Chemistry and Physics*, 8(19), 5755-5769.
- 422 Bondy, A. L., B. Wang, A. Laskin, R. L. Craig, M. V. Nhliziyo, S. B. Bertman, K. A. Pratt, P. B.
423 Shepson, and A. P. Ault (2017), Inland Sea Spray Aerosol Transport and Incomplete Chloride
424 Depletion: Varying Degrees of Reactive Processing Observed during SOAS, *Environmental Science*
425 *& Technology*, 51(17), 9533-9542.
- 426 Buseck, P. R., and M. Pósfai (1999), Airborne minerals and related aerosol particles: Effects on climate
427 and the environment, *Proceedings of the National Academy of Sciences*, 96(7), 3372-3379.
- 428 Chi, J. W., W. J. Li, D. Z. Zhang, J. C. Zhang, Y. T. Lin, X. J. Shen, J. Y. Sun, J. M. Chen, X. Y. Zhang,
429 Y. M. Zhang, and W. X. Wang (2015), Sea salt aerosols as a reactive surface for inorganic and
430 organic acidic gases in the Arctic troposphere, *Atmospheric Chemistry and Physics*, 15(19),
431 11341-11353.
- 432 Cravigan, L. T., M. D. Mallet, P. Vaattovaara, M. J. Harvey, C. S. Law, R. L. Modini, L. M. Russell, E.
433 Stelcer, D. D. Cohen, G. Olsen, K. Safi, T. J. Burrell, and Z. Ristovski (2020), Sea spray aerosol
434 organic enrichment, water uptake and surface tension effects, *Atmospheric Chemistry and Physics*,
435 20(13), 7955-7977.
- 436 Feng, J. L., Z. G. Guo, T. R. Zhang, X. H. Yao, C. K. Chan, and M. Fang (2012), Source and formation
437 of secondary particulate matter in PM_{2.5} in Asian continental outflow, *Journal of Geophysical*
438 *Research: Atmospheres*, 117, D03302.
- 439 Feng, L., H. Shen, Y. Zhu, H. Gao, and X. Yao (2017), Insight into Generation and Evolution of
440 Sea-Salt Aerosols from Field Measurements in Diversified Marine and Coastal Atmospheres,
441 *Scientific Reports*, 7, 41260.
- 442 Fu, J., B. Wang, Y. Chen, and Q. Ma (2018), The influence of continental air masses on the aerosols
443 and nutrients deposition over the western North Pacific, *Atmospheric Environment*, 172, 1-11.
- 444 Geng, H., J. Ryu, H.-J. Jung, H. Chung, K.-H. Ahn, and C.-U. Ro (2010), Single-Particle
445 Characterization of Summertime Arctic Aerosols Collected at Ny-Ålesund, Svalbard,
446 *Environmental Science & Technology*, 44(7), 2348-2353.
- 447 George, S. K., P. R. Nair, K. Parameswaran, S. Jacob, and A. Abraham (2008), Seasonal trends in
448 chemical composition of aerosols at a tropical coastal site of India, *Journal of Geophysical*
449 *Research: Atmospheres*, 113(D16), D16209.
- 450 Ghorai, S., B. Wang, A. Tivanski, and A. Laskin (2014), Hygroscopic Properties of Internally Mixed



- 451 Particles Composed of NaCl and Water-Soluble Organic Acids, *Environmental Science &*
452 *Technology*, 48(4), 2234-2241.
- 453 Guo, L., Y. Chen, F. Wang, X. Meng, Z. Xu, and G. Zhuang (2014), Effects of Asian dust on the
454 atmospheric input of trace elements to the East China Sea, *Marine Chemistry*, 163, 19-27.
- 455 He, X.-C., Y. J. Tham, L. Dada, M. Wang, H. Finkenzeller, D. Stolzenburg, S. Iyer, M. Simon, A.
456 Kürten, J. Shen, B. Rörup, M. Rissanen, S. Schobesberger, R. Baalbaki, D. S. Wang, T. K. Koenig,
457 T. Jokinen, N. Sarnela, L. J. Beck, J. Almeida, S. Amanatidis, A. Amorim, F. Ataci, A. Baccarini, B.
458 Bertozzi, F. Bianchi, S. Brilke, L. Caudillo, D. Chen, R. Chiu, B. Chu, A. Dias, A. Ding, J. Dommen,
459 J. Duplissy, I. El Haddad, L. Gonzalez Carracedo, M. Granzin, A. Hansel, M. Heinritzi, V. Hofbauer,
460 H. Junninen, J. Kangasluoma, D. Kemppainen, C. Kim, W. Kong, J. E. Krechmer, A. Kvashin, T.
461 Laitinen, H. Lamkaddam, C. P. Lee, K. Lehtipalo, M. Leiminger, Z. Li, V. Makhmutov, H. E.
462 Manninen, G. Marie, R. Marten, S. Mathot, R. L. Mauldin, B. Mentler, O. Möhler, T. Müller, W.
463 Nie, A. Onnela, T. Petäjä, J. Pfeifer, M. Philippov, A. Ranjithkumar, A. Saiz-Lopez, I. Salma, W.
464 Scholz, S. Schuchmann, B. Schulze, G. Steiner, Y. Stozhkov, C. Tauber, A. Tomé R. C. Thakur, O.
465 Väisänen, M. Vazquez-Pufleau, A. C. Wagner, Y. Wang, S. K. Weber, P. M. Winkler, Y. Wu, M.
466 Xiao, C. Yan, Q. Ye, A. Ylisirniö, M. Zauner-Wieczorek, Q. Zha, P. Zhou, R. C. Flagan, J. Curtius,
467 U. Baltensperger, M. Kulmala, V.-M. Kerminen, T. Kurtén, N. M. Donahue, R. Volkamer, J. Kirkby,
468 D. R. Worsnop, and M. Sipilä (2021), Role of iodine oxoacids in atmospheric aerosol nucleation,
469 *Science*, 371(6529), 589.
- 470 Hsu, S.-C., S. C. Liu, S.-J. Kao, W.-L. Jeng, Y.-T. Huang, C.-M. Tseng, F. Tsai, J.-Y. Tu, and Y. Yang
471 (2007), Water-soluble species in the marine aerosol from the northern South China Sea: High
472 chloride depletion related to air pollution, *Journal of Geophysical Research: Atmospheres*,
473 112(D19), D19304.
- 474 Hu, R. M., J. P. Blanchet, and E. Girard (2005), Evaluation of the direct and indirect radiative and
475 climate effects of aerosols over the western Arctic, *Journal of Geophysical Research: Atmospheres*,
476 110(D11), D11213.
- 477 Kang, M., P. Fu, K. Kawamura, F. Yang, H. Zhang, Z. Zang, H. Ren, L. Ren, Y. Zhao, Y. Sun, and Z.
478 Wang (2018), Characterization of biogenic primary and secondary organic aerosols in the marine
479 atmosphere over the East China Sea, *Atmospheric Chemistry and Physics*, 18(19), 13947-13967.
- 480 Koike, M., Y. Kondo, K. Kita, N. Takegawa, Y. Masui, Y. Miyazaki, M. W. Ko, A. J. Weinheimer, F.
481 Flocke, R. J. Weber, D. C. Thornton, G. W. Sachse, S. A. Vay, D. R. Blake, D. G. Streets, F. L.
482 Eisele, S. T. Sandholm, H. B. Singh, and R. W. Talbot (2003), Export of anthropogenic reactive
483 nitrogen and sulfur compounds from the East Asia region in spring, *Journal of Geophysical*
484 *Research: Atmospheres*, 108(D20), 8789.
- 485 Kondo, Y., N. Moteki, N. Oshima, S. Ohata, M. Koike, Y. Shibano, N. Takegawa, and K. Kita (2016),
486 Effects of wet deposition on the abundance and size distribution of black carbon in East Asia,
487 *Journal of Geophysical Research: Atmospheres*, 121(9), 4691-4712.
- 488 Laskin, A., R. C. Moffet, M. K. Gilles, J. D. Fast, R. A. Zaveri, B. Wang, P. Nigge, and J.
489 Shutthanandan (2012), Tropospheric chemistry of internally mixed sea salt and organic particles:
490 Surprising reactivity of NaCl with weak organic acids, *Journal of Geophysical Research:*
491 *Atmospheres*, 117(D15), D15302.
- 492 Lewis, E. R., and S. E. Schwartz (2004), *Sea salt aerosol production: mechanisms, methods,*
493 *measurements, and models*, American Geophysical Union, Washington, DC.
- 494 Li, W., L. Liu, J. Zhang, L. Xu, Y. Wang, Y. Sun, and Z. Shi (2021), Microscopic Evidence for Phase



- 495 Separation of Organic Species and Inorganic Salts in Fine Ambient Aerosol Particles,
496 *Environmental Science & Technology*, 55(4), 2234-2242.
- 497 Li, W., L. Shao, D. Zhang, C.-U. Ro, M. Hu, X. Bi, H. Geng, A. Matsuki, H. Niu, and J. Chen (2016a),
498 A review of single aerosol particle studies in the atmosphere of East Asia: morphology, mixing state,
499 source, and heterogeneous reactions, *Journal of Cleaner Production*, 112, Part 2, 1330-1349.
- 500 Li, W., L. Shao, Z. Shi, J. Chen, L. Yang, Q. Yuan, C. Yan, X. Zhang, Y. Wang, J. Sun, Y. Zhang, X.
501 Shen, Z. Wang, and W. Wang (2014), Mixing state and hygroscopicity of dust and haze particles
502 before leaving Asian continent, *Journal of Geophysical Research: Atmospheres*, 119(2), 1044-1059.
- 503 Li, W., J. Sun, L. Xu, Z. Shi, N. Riemer, Y. Sun, P. Fu, J. Zhang, Y. Lin, X. Wang, L. Shao, J. Chen, X.
504 Zhang, Z. Wang, and W. Wang (2016b), A conceptual framework for mixing structures in individual
505 aerosol particles, *Journal of Geophysical Research: Atmospheres*, 121(22), 13784-13798.
- 506 Li, W., L. Xu, X. Liu, J. Zhang, Y. Lin, X. Yao, H. Gao, D. Zhang, J. Chen, W. Wang, R. M. Harrison,
507 X. Zhang, L. Shao, P. Fu, A. Nenes, and Z. Shi (2017), Air pollution–aerosol interactions produce
508 more bioavailable iron for ocean ecosystems, *Science Advances*, 3(3), e1601749.
- 509 Luo, L., X. H. Yao, H. W. Gao, S. C. Hsu, J. W. Li, and S. J. Kao (2016), Nitrogen speciation in various
510 types of aerosols in spring over the northwestern Pacific Ocean, *Atmospheric Chemistry and
511 Physics*, 16(1), 325-341.
- 512 Mahowald, N. M., D. S. Hamilton, K. R. M. Mackey, J. K. Moore, A. R. Baker, R. A. Scanza, and Y.
513 Zhang (2018), Aerosol trace metal leaching and impacts on marine microorganisms, *Nature
514 communications*, 9(1), 2614.
- 515 McInnes, L. M., D. S. Covert, P. K. Quinn, and M. S. Germani (1994), Measurements of chloride
516 depletion and sulfur enrichment in individual sea-salt particles collected from the remote marine
517 boundary layer, *Journal of Geophysical Research: Atmospheres*, 99(D4), 8257-8268.
- 518 Moffet, R. C., H. Furutani, T. C. Rödel, T. R. Henn, P. O. Sprau, A. Laskin, M. Uematsu, and M. K.
519 Gilles (2012), Iron speciation and mixing in single aerosol particles from the Asian continental
520 outflow, *Journal of Geophysical Research: Atmospheres*, 117(D7), D07204.
- 521 Mouri, H., and K. Okada (1993), Shattering and modification of sea-salt particles in the marine
522 atmosphere, *Geophysical Research Letters*, 20(1), 49-52.
- 523 Murphy, D., J. Anderson, P. Quinn, L. McInnes, F. Brechtel, S. Kreidenweis, A. Middlebrook, M.
524 Pósfai, D. Thomson, and P. Buseck (1998), Influence of sea-salt on aerosol radiative properties in
525 the Southern Ocean marine boundary layer, *Nature*, 392, 62-65.
- 526 O'Dowd Colin, D., and G. de Leeuw (2007), Marine aerosol production: a review of the current
527 knowledge, *Philosophical Transactions of the Royal Society A: Mathematical, Physical and
528 Engineering Sciences*, 365(1856), 1753-1774.
- 529 Pósfai, M., J. R. Anderson, P. R. Buseck, T. W. Shattuck, and N. W. Tindale (1994), Constituents of a
530 remote pacific marine aerosol: A tem study, *Atmospheric Environment*, 28(10), 1747-1756.
- 531 Pant, V., C. G. Deshpande, and A. K. Kamra (2008), On the aerosol number concentration–wind speed
532 relationship during a severe cyclonic storm over south Indian Ocean, *Journal of Geophysical
533 Research: Atmospheres*, 113(D2), D02206.
- 534 Pierce, J. R., and P. J. Adams (2006), Global evaluation of CCN formation by direct emission of sea
535 salt and growth of ultrafine sea salt, *Journal of Geophysical Research: Atmospheres*, 111(D6),
536 D06203.
- 537 Quinn, P. K., T. S. Bates, J. E. Johnson, D. S. Covert, and R. J. Charlson (1990), Interactions between
538 the sulfur and reduced nitrogen cycles over the central Pacific Ocean, *Journal of Geophysical*



- 539 *Research: Atmospheres*, 95(D10), 16405-16416.
- 540 Riemer, N., A. P. Ault, M. West, R. L. Craig, and J. H. Curtis (2019), Aerosol Mixing State:
541 Measurements, Modeling, and Impacts, *Reviews of Geophysics*, 57(2), 187-249.
- 542 Savoie, D. L., J. M. Prospero, R. Arimoto, and R. A. Duce (1994), Non-sea-salt sulfate and
543 methanesulfonate at American Samoa, *Journal of Geophysical Research: Atmospheres*, 99(D2),
544 3587-3596.
- 545 Shi, J., N. Wang, H. Gao, A. R. Baker, X. Yao, and D. Zhang (2019), Phosphorus solubility in aerosol
546 particles related to particle sources and atmospheric acidification in Asian continental outflow,
547 *Atmospheric Chemistry and Physics*, 19(2), 847-860.
- 548 Shi, Z., M. D. Krom, T. D. Jickells, S. Bonneville, K. S. Carslaw, N. Mihalopoulos, A. R. Baker, and L.
549 G. Benning (2012), Impacts on iron solubility in the mineral dust by processes in the source region
550 and the atmosphere: A review, *Aeolian Research*, 5, 21-42.
- 551 Shinozuka, Y., A. D. Clarke, S. G. Howell, V. N. Kapustin, and B. J. Huebert (2004), Sea-salt vertical
552 profiles over the Southern and tropical Pacific oceans: Microphysics, optical properties, spatial
553 variability, and variations with wind speed, *Journal of Geophysical Research: Atmospheres*,
554 109(D24), D24201.
- 555 Sievering, H., J. Caniney, M. Harvey, J. McGregor, S. Nichol, and P. Quinn (2004), Aerosol non-sea-salt
556 sulfate in the remote marine boundary layer under clear-sky and normal cloudiness conditions:
557 Ocean-derived biogenic alkalinity enhances sea-salt sulfate production by ozone oxidation, *Journal*
558 *of Geophysical Research: Atmospheres*, 109(D19), D19317.
- 559 Ueda, S., K. Osada, K. Hara, M. Yabuki, F. Hashihama, and J. Kanda (2018), Morphological features
560 and mixing states of soot-containing particles in the marine boundary layer over the Indian and
561 Southern oceans, *Atmospheric Chemistry and Physics*, 18(13), 9207-9224.
- 562 Uematsu, M., H. Hattori, T. Nakamura, Y. Narita, J. Jung, K. Matsumoto, Y. Nakaguchi, and M. D.
563 Kumar (2010), Atmospheric transport and deposition of anthropogenic substances from the Asia to
564 the East China Sea, *Marine Chemistry*, 120(1), 108-115.
- 565 Uno, I., K. Eguchi, K. Yumimoto, T. Takemura, A. Shimizu, M. Uematsu, Z. Liu, Z. Wang, Y. Hara, and
566 N. Sugimoto (2009), Asian dust transported one full circuit around the globe, *Nature geoscience*,
567 2(8), 557-560.
- 568 Wang, J., J. Ye, Q. Zhang, J. Zhao, Y. Wu, J. Li, D. Liu, W. Li, Y. Zhang, C. Wu, C. Xie, Y. Qin, Y. Lei,
569 X. Huang, J. Guo, P. Liu, P. Fu, Y. Li, H. C. Lee, H. Choi, J. Zhang, H. Liao, M. Chen, Y. Sun, X.
570 Ge, S. T. Martin, and D. J. Jacob (2021), Aqueous production of secondary organic aerosol from
571 fossil-fuel emissions in winter Beijing haze, *Proceedings of the National Academy of Sciences*,
572 118(8), e2022179118.
- 573 Wang, Z., L. Bi, B. Yi, and X. Zhang (2019), How the Inhomogeneity of Wet Sea Salt Aerosols Affects
574 Direct Radiative Forcing, *Geophysical Research Letters*, 46(3), 1805-1813.
- 575 Yao, X., and L. Zhang (2012), Chemical processes in sea-salt chloride depletion observed at a Canadian
576 rural coastal site, *Atmospheric Environment*, 46, 189-194.
- 577 Yu, H., L. Ren, X. Huang, M. Xie, J. He, and H. Xiao (2019), Iodine speciation and size distribution in
578 ambient aerosols at a coastal new particle formation hotspot in China, *Atmospheric Chemistry and*
579 *Physics*, 19(6), 4025-4039.
- 580 Zhang, D., Y. Iwasaka, G. Shi, J. Zang, A. Matsuki, and D. Trochkin (2003), Mixture state and size of
581 Asian dust particles collected at southwestern Japan in spring 2000, *Journal of Geophysical*
582 *Research: Atmospheres*, 108(D24), 4760.



583 Zhang, X., P. Massoli, P. K. Quinn, T. S. Bates, and C. D. Cappa (2014), Hygroscopic growth of
584 submicron and supermicron aerosols in the marine boundary layer, *Journal of Geophysical*
585 *Research: Atmospheres*, 119(13), 8384-8399.

586 Zhang, X. X., B. Sharratt, L. Y. Liu, Z. F. Wang, X. L. Pan, J. Q. Lei, S. X. Wu, S. Y. Huang, Y. H. Guo,
587 J. Li, X. Tang, T. Yang, Y. Tian, X. S. Chen, J. Q. Hao, H. T. Zheng, Y. Y. Yang, and Y. L. Lyu
588 (2018), East Asian dust storm in May 2017: observations, modelling, and its influence on the
589 Asia-Pacific region, *Atmospheric Chemistry and Physics*, 18(11), 8353-8371.

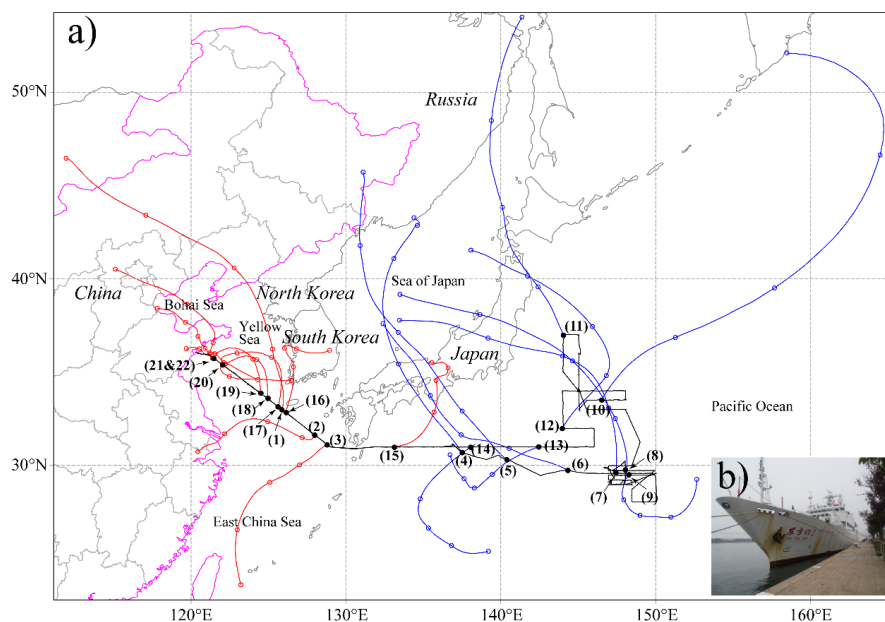
590 Zhu, Y., K. Li, Y. Shen, Y. Gao, X. Liu, Y. Yu, H. Gao, and X. Yao (2019), New particle formation in
591 the marine atmosphere during seven cruise campaigns, *Atmospheric Chemistry and Physics*, 19(1),
592 89-113.

593

594



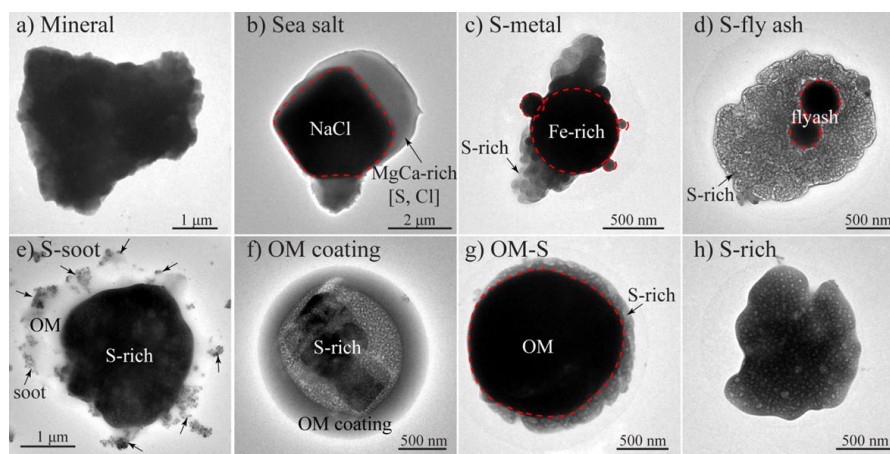
595 **Figures**



596

597 Figure 1. (a) Map of the cruise track (black line) and 48 h air mass backward
598 trajectories (red and blue lines) arriving at 500 m above ground level at sampling
599 locations. The interval between two circle symbols is 6 h. The number represents the
600 sample ID in Table S1. (b) Photo of the R/V Dongfanghong 2.

601

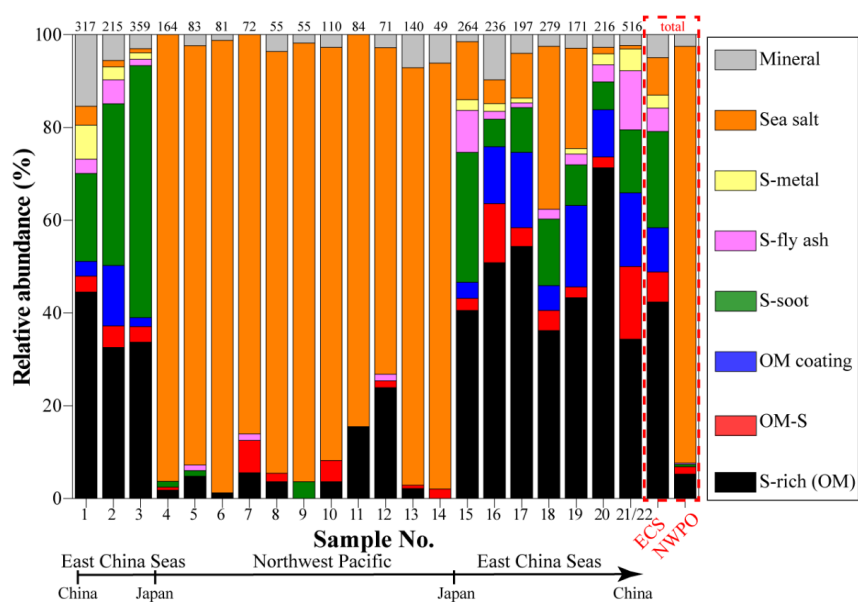


602



603 Figure 2. Transmission electron microscope (TEM) images of different types of
604 aerosol particles: (a) mineral; (b) sea salt; (c) metal particles mixed with sulfate; (d)
605 fly ash particles mixed with sulfate; (e) soot particles mixed with sulfate; (f)
606 secondary organic matter (OM) coating on sulfate; (g) primary OM particle mixed
607 with sulfate; (h) S-rich particle.

608

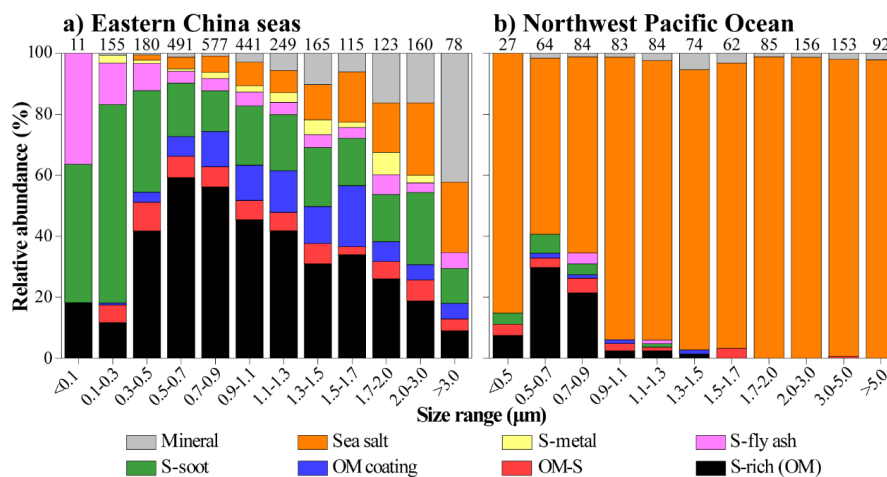


609

610 Figure 3. Relative abundances of eight types of aerosol particles in different samples.

611 The number of analyzed aerosol particles is shown above the column.

612

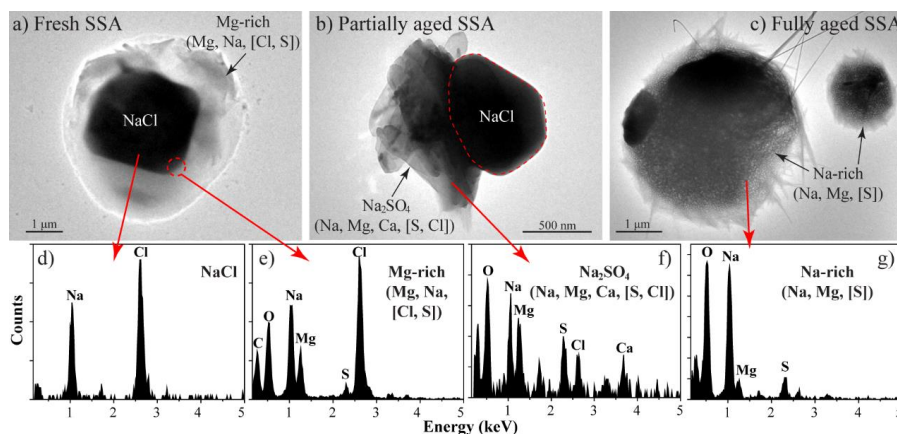


613

614

Figure 4. Relative abundances of individual particles in different size bins.

615

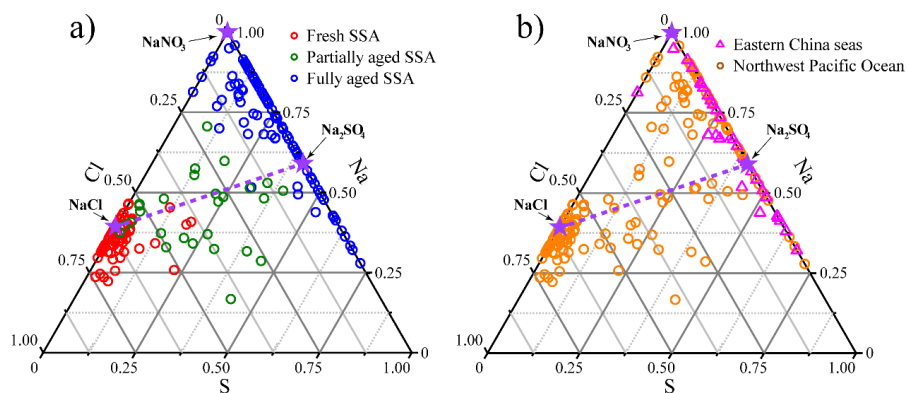


616

Figure 5. Morphology and EDS spectra of the typical fresh, partially aged, and fully aged SSA. The main anionic elements are shown in the square brackets.

618

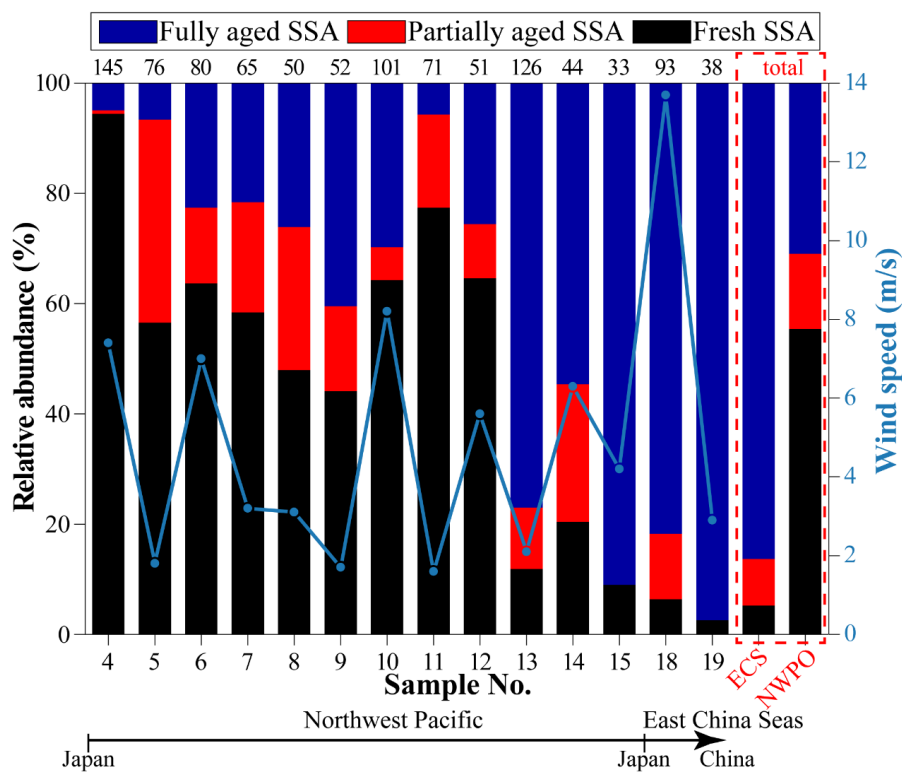
619



620

621 Figure 6. Triangular diagram of Na-Cl-S from EDS data (weight percentage) showing
622 the elemental composition of SSA particles. The three stars represent pure NaCl,
623 Na₂SO₄, and NaNO₃, respectively. The dash line indicates that Na:Cl:S is changed
624 only by the postulated reaction of $2\text{NaCl} + \text{H}_2\text{SO}_4 \rightarrow \text{Na}_2\text{SO}_4 + 2\text{HCl}(\text{g})$ (Zhang et
625 al., 2003). Particles above the dash line are those which S cannot compensate Cl
626 losses and there should be other processes causing Cl-depletion.

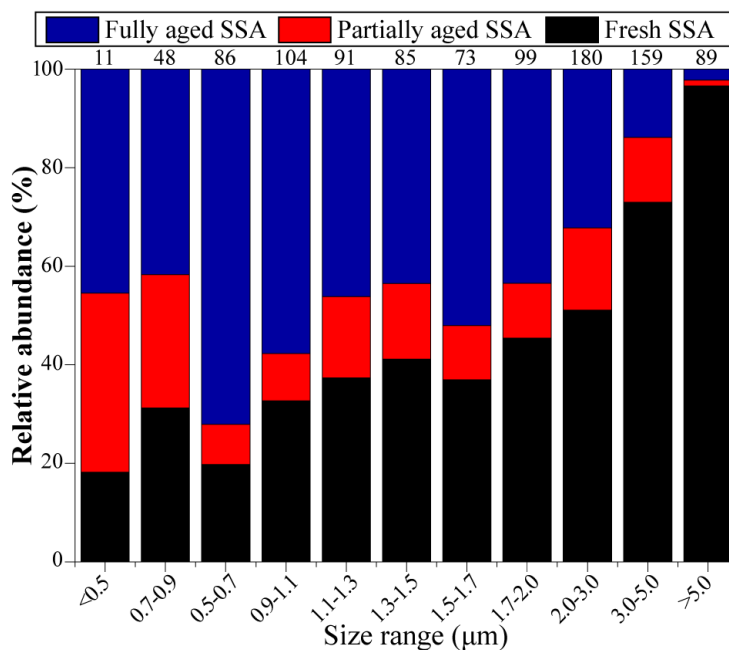
627



628

629 Figure 7. Relative abundances of the fresh, partially aged, and fully aged SSA
 630 particles in different samples. Samples with SSA particle less than 30 are excluded
 631 due to the small number. The line indicates the wind speed of the corresponding
 632 sample.

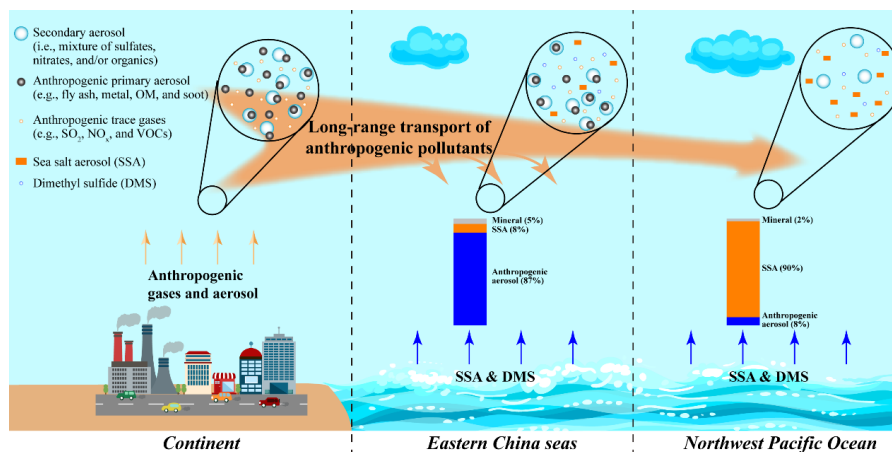
633



634

635 Figure 8. Relative abundances of three types of SSA particles in different size bins

636



637

638 Figure 9. Schematic diagram showing the impact of long-range transported

639 anthropogenic air pollutants on marine aerosols

640